Electronic supplementary information

Solvent Engineering for Achieving Six Copper-Based Halides from a Single Organic Cation: Full-colour Luminescence and Multimode-Stimulus Response

Junyan Wu,[a, +] Wanxin Shi,[a, +] Yuechuan Wu,[a] Shilin Jin,[b] Zhenzhu Liu,[a] daqin Chen,[b] Zhenghuan Lin[a, *]

[a] *Fujian Key Laboratory of Polymer Materials, College of Chemistry and Materials Science, Fujian Normal University, Fuzhou, 350007, China*

[b] *College of Physics and Energy, Fujian Normal University, Fuzhou, 350117, China*

[+] These authors contributed equally to this work.

Email: zhlin@fjnu.edu.cn

Experimental section

Measurements

The crystalline structure of the samples was analyzed by Powder X-ray diffraction using a PANalytical X-ray Diffractometer (X'Pert3 Powder) with Cu Kα radiation (λ = 1.54178 Å) with a step size of 10°/min. Steady-state photoluminescence spectra of the samples were obtained at room temperature using an Edinburgh FS5 spectrofluorometer equipped with a xenon arc lamp (Xe900). Time-resolved photoluminescence decay curves were recorded using an FLS920 fluorescence spectrometer equipped with a nanosecond flash lamp (nF900). UV-visible absorption spectra were measured using a PerkinElmer LAMBDA750S spectrophotometer. TGA was obtained using Mettler's thermogravimeter.

Materials

Trans-1,4-diaminocyclohexane (98%), CuI (99.5%), and acetonitrile (99.5%) were purchased from Tansoole Company, Aladdin Company, and Sinopharm Chemical Reagent Co., Ltd., respectively. H_3PO_2 (50 wt%) and HI (47.0%) were both obtained from Macklin Company. All commercial reagents were used directly without further purification.

Synthesis of N. A mixture containing trans-1,4-cyclohexanediamine (1 mmol, 114 mg), CuI (2 mmol, 380.9 mg), HI (6.25 mol/L, 0.5 mL), H_3PO_2 (10.9 mol/L, 0.5 mL), and 1 mL of acetonitrile was sealed in a 25 mL Teflon-lined autoclave. The reaction was carried out at 120 °C for 8 hours, followed by slow cooling to room temperature. After filtered and dried at 45°C under vacuum, **N** was obtained in colorless crystals with a yield of approximately 36.4%.

Synthesis of C. A mixture of trans-1,4-cyclohexanediamine (0.5 mmol, 57 mg), CuI (1 mmol, 190.45 mg), HI (6.25 mol/L, 0.2 mL), H_3PO_2 (10.9 mol/L, 0.5 mL) , and 1 mL of acetonitrile was stirred and heated at 85 °C for 20 min. After cooling to room temperature, the solution was added 2 mg **C** seed crystals, and slowly volatilized to give **C** in colorless crystals, followed by filtration and blotted dry with filter paper for further use. The yield was approximately 60.3%. The **C** seed crystals were obtained by

immersing **N** in acetonitrile.

Synthesis of B. A mixture containing trans-1,4-cyclohexanediamine (1 mmol, 114 mg), CuI (2 mmol, 380.9 mg), HI (6.25 mol/L, 1 mL), H_3PO_2 (10.9 mol/L, 0.5 mL), and 1 mL of acetonitrile was sealed in a 25 mL Teflon-lined autoclave. The reaction was carried out at 120 °C for 8 hours, followed by slow cooling to room temperature. After filtered and dried at 45°C under vacuum, **B** was obtained in colorless crystals with a yield of approximately 51.3%.

Synthesis of G. A mixture of trans-1,4-cyclohexanediamine (0.5 mmol, 57 mg), CuI (1 mmol, 190.45 mg), HI (6.25 mol/L, 0.5 mL), H_2O (0.2 mL), H_3PO_2 (10.9 mol/L, 0.5 mL), and 1 mL of acetonitrile was heated at 85 °C for 20 min with stirring, followed by slow cooling to room temperature. After filtered and dried with filter paper, **G** was obtained in colorless crystals with a yield of approximately 37.2%.

Synthesis of Y. A mixture of trans-1,4-cyclohexanediamine (1 mmol, 114 mg), CuI (2 mmol, 380.9 mg), HI (6.25 mol/L, 0.6 mL), H_3PO_2 (10.9 mol/L, 0.5 mL), and 0.5 mL of acetonitrile was sealed in a 25 mL Teflon-lined autoclave and heated at 120 °C for 8 h, followed by slow cooling to room temperature. After filtered and dried at 45°C under vacuum, **Y** was obtained in colorless crystals with a yield of approximately 56.7%.

Synthesis of R. First, trans-1,4-cyclohexanediamine hydroiodide was prepared as an intermediate. trans-1,4-cyclohexanediamine (15 mmol, 1.71 g) was dissolved in 10 mL of ethanol in a 250 mL pear-shaped flask, followed by the addition of HI (6.25 mol/L, 5 mL). The mixture was stirred at room temperature for 12 h. The solvent was then removed under reduced pressure to afford a brown crude solid, which was recrystallized via liquid diffusion using ethanol and ethyl acetate to give the purified hydroiodide salt.

Then, the intermediate trans-1,4-cyclohexanediamine hydroiodide (0.4 mmol, 147 mg) and CuI (0.2 mmol, 38.09 mg) were dissolved in a mixed solvent of acetonitrile (1 mL) and H_2O (0.2 mL). The solution was stirred and heated at 85 °C for 20 min, followed by slow cooling to room temperature. After filtered and dried at 45°C under vacuum, **R** was obtained in brown crystals with a yield of approximately 50.5%.

X-ray crystallography

The single crystals of **N**, **B**, **C**, **G**, **Y** and **R** were mounted on a glass fiber for the X-ray diffraction analysis. Single crystal X-ray diffraction data was collected on an Agilent Technologies SuperNova single-crystal diffractometer equipped with graphite monochromatic Cu *Kα* radiation (λ = 1.54184 Å). Using Olex2 software, the structure was solved with the SHELXT structure solution program using Intrinsic Phasing and refined with the SHELXL refinement package using Least Squares minimization. The detailed crystallographic data and structure refinement parameters were summarized in Table S1-S2.

Theoretical calculation

First-principles calculations were performed using Vienna ab initio simulation package (VASP) to obtain the electronic band structures and partial density of states with the aid of VASPKIT.[1, 2] Electron–ion interaction was described by the projector augmented wave (PAW) pseudopotentials and exchange-correlation interactions were described by the generalized gradient approximation (GGA) with Perdew-Burke-Ernzerh (PBE) function.[3] During structural optimization, a Gamma centered Monkhorst–Pack k-point grid of 2 × 1 × 1 and 4 × 1 × 3 was employed to sample the Brillouin zone of **G** and **Y**, respectively. The energy cut-off for the plane wave basis expansion was set to 400 eV.

The force and energy convergence criteria were set to be 0.01 eV $Å^{-1}$ and 10^{-6} eV, respectively. The DFT-D3 method developed by Grimme was employed to treat the Van der Waals interactions.

Calculation formula

Tetrahedral bond-length distortion index Δd:[4]

$$\Delta d = 1/4 \sum_{i=1}^{4} \left(\frac{d_i - d_0}{d_0} \right)^2 \qquad (1)$$

Where d_0 is the average bond length of the Cu–I bonds, and d_i is the bond length of an individual Cu–I bond.

The formula for calculating the Huang-Rhys factor:[5]

$$FWHM = 2.36\sqrt{s}\hbar\omega_{photon}\sqrt{\coth\frac{\hbar\omega_{photon}}{2\kappa_B T}} \qquad (2)$$

Where FWHM is the full width at half maximum of the emission spectrum, $\hbar\omega_{phonon}$ is the phonon energy, and κ_B is the Boltzmann constant.

Arrhenius equation:[6]

$$I(T) = \frac{I_0}{1 + Aexp(\frac{-E_a}{\kappa_B T})} \qquad (3)$$

Where I_0 is the PL intensity at 0 K, I(T) is the PL intensity at temperature T, A is a constant, and E_a is the activation energy.

Table S1. Crystal data and structure refinements for compound **N**，**B** and **C**.

Compound	**N**	**B**	**C**
Empirical formula	$C_{12}H_{32}Cu_4I_8N_4$	$C_6H_{22}Cu_2I_6N_2O_2$	$C_{10}Cu_2I_4N_4H_{22}$
Formula weight	1501.77	1042.73	832.99
Temperature/K	295.95(10)	297.02(11)	100.00(10)
Crystal system	orthorhombic	monoclinic	triclinic
Space group	*Pbcn*	$P2_1/c$	*P*-1
a(Å)	15.253(2)	9.7943(16)	7.5688(3)
b(Å)	15.572(2)	13.393(2)	8.6779(3)
c(Å)	13.4275(17)	8.6387(13)	9.1991(3)
α (deg)	90	90	71.698(3)
β(deg)	90	96.410(15)	70.287(3)
γ(deg)	90	90	68.046(3)
Volume(Å^3)	3189.3(8)	1126.1(3)	515.19(4)
Z	4	2	1
R_1	0.0445	0.0526	0.0586
wR_2	0.0944	0.1233	0.1727
CCDC No.	2513889	2513886	2513887

Table S2. Crystal data and structure refinements for compound **G**，**Y** and **R**.

Compound	**G**	**Y**	**R**
Empirical formula	$C_{12}H_{36}Cu_3I_7N_4O_2$	$C_6H_{19}Cu_3I_6N_2O$	$C_6H_{14}Cu_2I_2N_2$
Formula weight	1347.37	1087.25	495.07
Temperature/K	100.00(10)	297.35(10)	301.25(10)
Crystal system	orthorhombic	monoclinic	monoclinic
Space group	*Pbca*	$P2_1/m$	$P2/n$
a(Å)	19.8679(3)	7.0507(8)	11.0998(4)
b(Å)	15.2152(2)	19.658(2)	7.8171(2)
c(Å)	19.9691(3)	8.0843(10)	14.6656(5)
α (deg)	90	90	90
β(deg)	90	108.581(13)	110.194(4)
γ(deg)	90	90	90
Volume(Å^3)	6036.54(15)	1062.1(2)	1194.29(7)
Z	8	2	4
R_1	0.0338	0.0389	0.0735
wR_2	0.0902	0.0825	0.2153
CCDC No.	2513888	2513891	2513890

Table S3. Bond distance (Å) and bond angle (°) of **N**.

Atom	Atom	Length/Å	Atom	Atom	Atom	Angle/°
I1	Cu1	2.6690(17)	I4	Cu1	I2	114.57(6)
I1	Cu2	2.6695(16)	I4	Cu1	I1	103.59(5)
I2	Cu1	2.6506(17)	I2	Cu1	I1	111.83(6)
I2	Cu2[1]	2.6608(17)	I4	Cu1	I3	114.19(6)
I3	Cu1	2.6795(17)	I2	Cu1	I3	100.05(5)
I3	Cu2[1]	2.6995(17)	I1	Cu1	I3	113.02(6)
I4	Cu1	2.6311(17)	I4	Cu2	I2[2]	115.48(6)
I4	Cu2	2.6438(16)	I4	Cu2	I1	103.23(5)
			I2[2]	Cu2	I1	115.58(6)
			I4	Cu2	I3[2]	112.40(6)
			I2[2]	Cu2	I3[2]	99.28(5)
			I1	Cu2	I3[2]	111.23(6)

Symmetry codes: [1] 1/2-*x*, 3/2-*y*, -1/2+*z*; [2] 1-*x*, 1-*y*, 1-*z*; [3] -*x*, +*y*, 1/2-*z*

Table S4. Bond distance (Å) and bond angle (°) of **B**.

Atom	**Atom**	**Length/Å**	**Atom**	**Atom**	**Atom**	**Angle/°**
I2	Cu1	2.6671(17)	I1	Cu1	I2	107.79(7)
I2	Cu1[1]	2.7549(19)	I1	Cu1	I2[1]	101.24(6)
I1	Cu1	2.6171(19)	I1	Cu1	I3	119.83(7)
I3	Cu1	2.6371(19)	I3	Cu1	I2[1]	103.26(6)
Cu1	Cu1[1]	2.743(3)	I3	Cu1	I2	106.24(6)
I2	Cu1	2.6671(17)				
I2	Cu1[1]	2.7549(19)				
I1	Cu1	2.6171(19)				

Symmetry codes: [1] 2-*x*, 1-*y*, 1-*z*; [2] 1-*x*, 1-*y*, -*z*

Table S5. Bond distance (Å) and bond angle (°) of **C**.

Atom	**Atom**	**Length/Å**	**Atom**	**Atom**	**Atom**	**Angle/°**
I2	Cu1[1]	2.6642(15)	I2[1]	Cu1	I2	119.58(6)
I2	Cu1	2.6689(16)	I1	Cu1	I2	110.28(6)
I1	Cu1	2.6366(17)	I1	Cu1	I2[1]	103.24(5)
Cu1	Cu1[1]	2.684(3)	N2	Cu1	I2[1]	109.6(2)
Cu1	N2	1.993(9)	N2	Cu1	I2	101.9(3)
			N2	Cu1	I1	112.6(3)

Symmetry codes: [1] 1-*x*, -*y*, -*z*; [2] -*x*, 1-*y*, 1-*z*

Table S6. Bond distance (Å) and bond angle (°) of **G**.

Atom	Atom	Length/Å	Atom	Atom	Atom	Angle/°
I3	Cu3	2.7040(9)	I3	Cu3	I7	106.75(3)
I4	Cu3	2.6301(9)	I4	Cu3	I3	101.49(3)
I4	Cu2	2.6440(10)	I4	Cu3	I7	117.54(3)
I6	Cu2	2.6519(10)	I2	Cu3	I3	111.11(3)
I6	Cu1	2.6100(9)	I2	Cu3	I4	115.28(3)
I7	Cu3	2.7068(9)	I2	Cu3	I7	104.46(3)
I7	Cu2	2.7630(10)	I4	Cu2	I6	112.01(3)
I7	Cu1	2.7203(10)	I4	Cu2	I7	115.12(3)
I2	Cu3	2.6257(9)	I6	Cu2	I7	106.04(3)
I2	Cu1	2.6200(9)	I5	Cu2	I4	106.09(3)
I5	Cu2	2.6404(9)	I5	Cu2	I6	116.13(3)
I1	Cu1	2.6464(10)	I5	Cu2	I7	101.27(3)
Cu3	Cu2	2.6742(12)	I6	Cu1	I7	108.49(3)
Cu3	Cu1	2.9175(13)	I6	Cu1	I2	117.65(4)
Cu2	Cu1	2.9259(13)	I6	Cu1	I1	112.95(3)
			I2	Cu1	I7	104.24(3)
			I2	Cu1	I1	106.13(3)
			I1	Cu1	I7	106.54(3)

Table S7. Bond distance (Å) and bond angle (°) of **Y**.

Atom	Atom	Length/Å	Atom	Atom	Atom	Angle/°
I3	Cu2	2.6245(9)	I3	Cu2	I3[1]	121.52(6)
I3	Cu1	2.5943(13)	I3	Cu2	I1	107.94(4)
I1	Cu2	2.6679(17)	I3[1]	Cu2	I1	107.94(4)
I1	Cu1[1]	2.9566(15)	I3	Cu2	I4[3]	101.30(4)
I1	Cu1	2.9566(15)	I3[1]	Cu2	I4[3]	101.30(4)
I2	Cu1	2.6011(12)	I1	Cu2	I4[3]	117.26(6)
I4	Cu2[2]	2.7652(19)	I3	Cu1	I1	100.69(4)
I4	Cu1	2.5968(12)	I3	Cu1	I2	115.45(4)
I4	Cu1[1]	2.5967(12)	I3	Cu1	I4	111.77(5)
Cu2	Cu1	2.9139(19)	I2	Cu1	I1	98.33(4)
Cu2	Cu1[1]	2.9139(19)	I4	Cu1	I1	118.56(4)
Cu1	Cu1[1]	2.754(2)	I4	Cu1	I2	111.29(5)

Symmetry codes: [1] +*x*, 1/2-*y*, +*z*; [2] -1+*x*, +*y*, +*z*; [3] 2-*x*, 1-*y*, 2-*z*

Table S8. Bond distance (Å) and bond angle (°) of **R**.

Atom	Atom	Length/Å	Atom	Atom	Atom	Angle/°
I2	Cu1[1]	2.713(3)	I2[1]	Cu1	I2	109.63(10)
I2	Cu1	2.745(3)	I1	Cu1	I2[1]	108.92(10)
I2	Cu2	2.740(3)	I1	Cu1	I2	119.96(10)
I1	Cu1	2.695(3)	I1	Cu2	I2	119.41(11)
I1	Cu2	2.715(3)	I1[1]	Cu2	I2	108.34(10)
I1	Cu2[1]	2.687(3)	I1[1]	Cu2	I1	112.27(10)
Cu1	Cu1[1]	2.780(5)				
Cu1	Cu2[1]	2.743(4)				
Cu2	Cu2[1]	2.662(5)				

Symmetry codes: [1] 3/2-*x*, +*y*, 1/2-*z*; [2] 1-*x*, -*y*, 1-*z*; [3] 1/2-*x*, +*y*, 1/2-*z*

Table S9. The bond length distortion parameters for the inorganic polyhedra in compounds **B**, **C**, **G**, **Y**, **N**, and **R.**

Compounds	Δd
N	5.72×10^{-5}
B	3.89×10^{-4}
C	1.33×10^{-2}
G	3.65×10^{-4}
Y	3.35×10^{-3}
R	1.32×10^{-2}

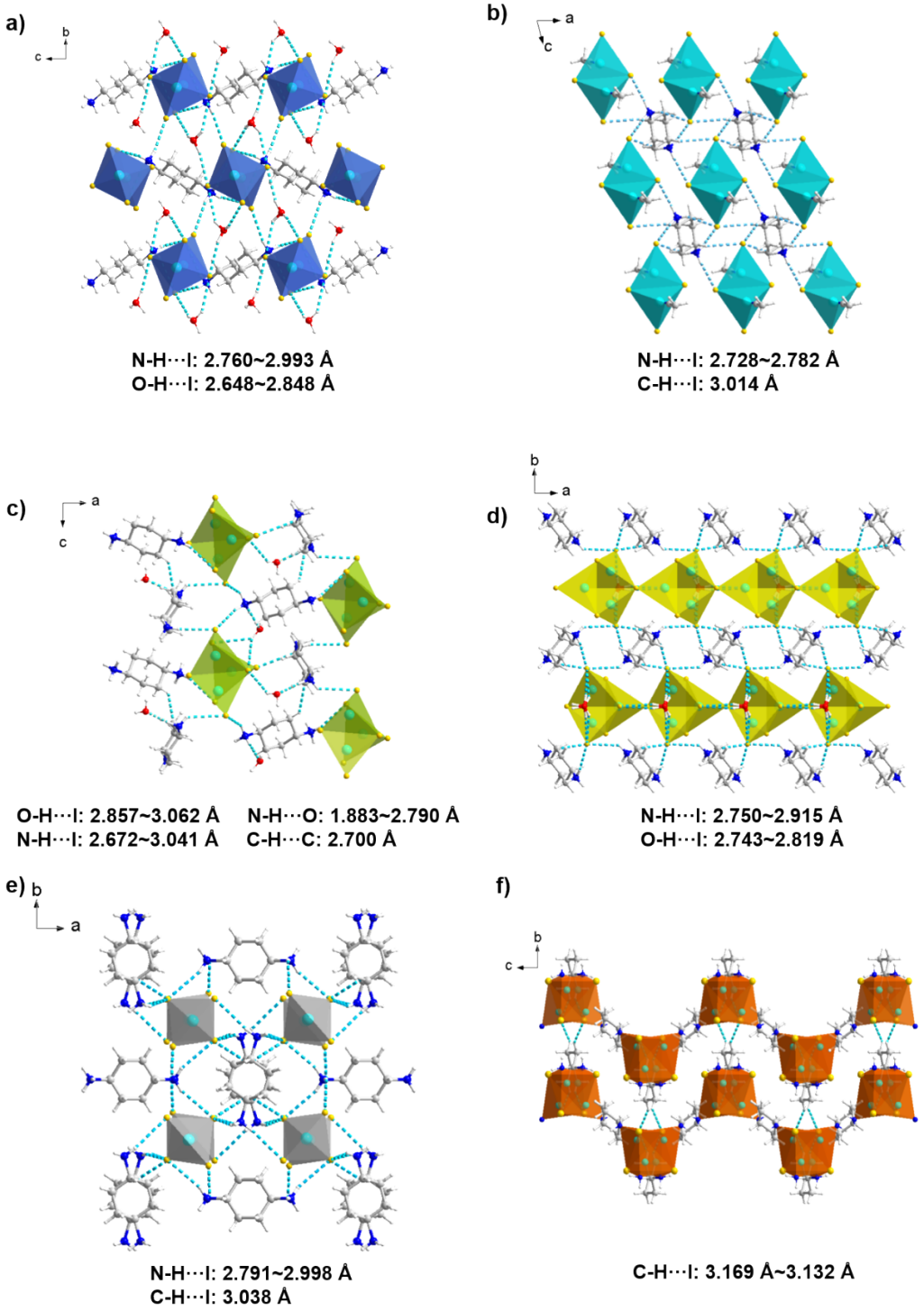

Fig. S1 Hydrogen bonding in a) **B**, b) **C**, c) **G**, d) **Y**, e) **N** and f) **R** molecules, represented by dashed lines.

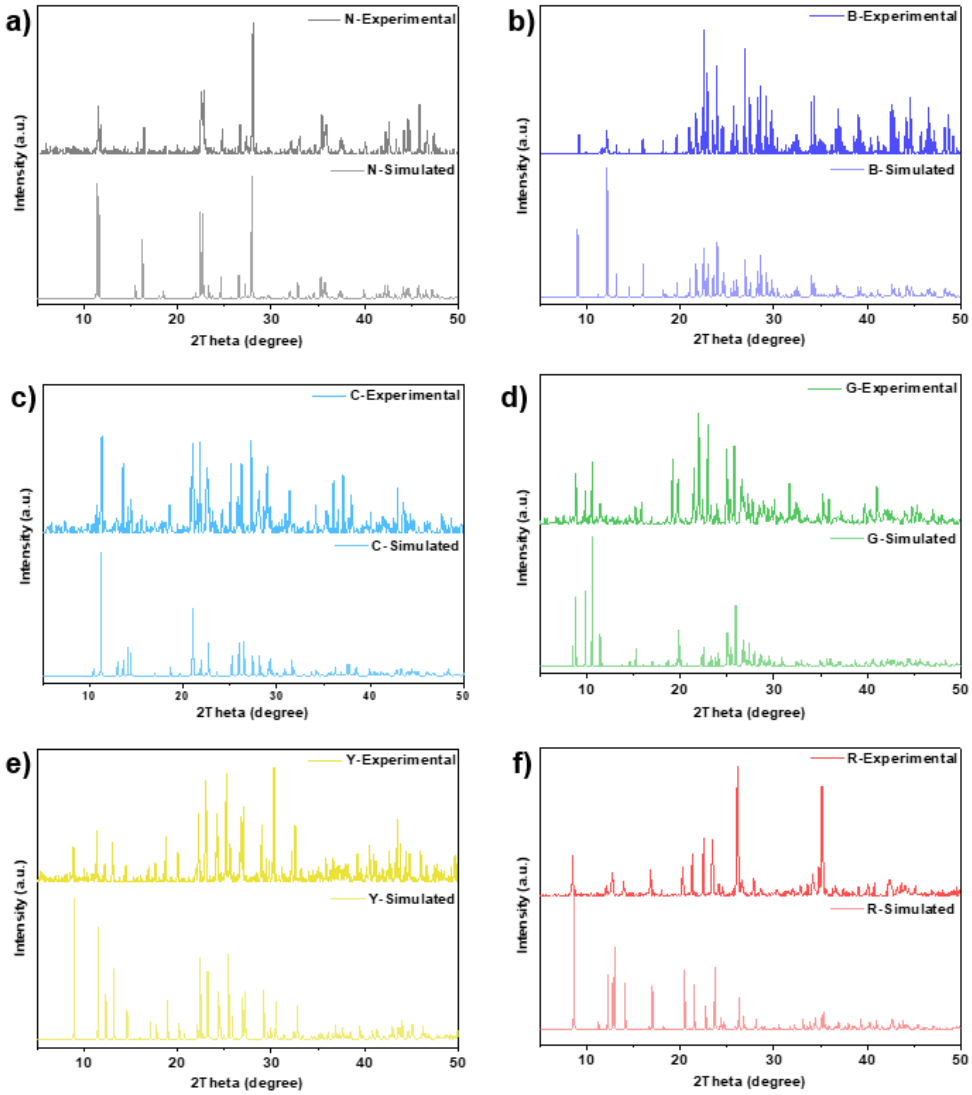

Fig. S2 PXRD patterns of a) **N**, b) **B**, c) **C**, d) **G**, e) **Y** and f) **R**.

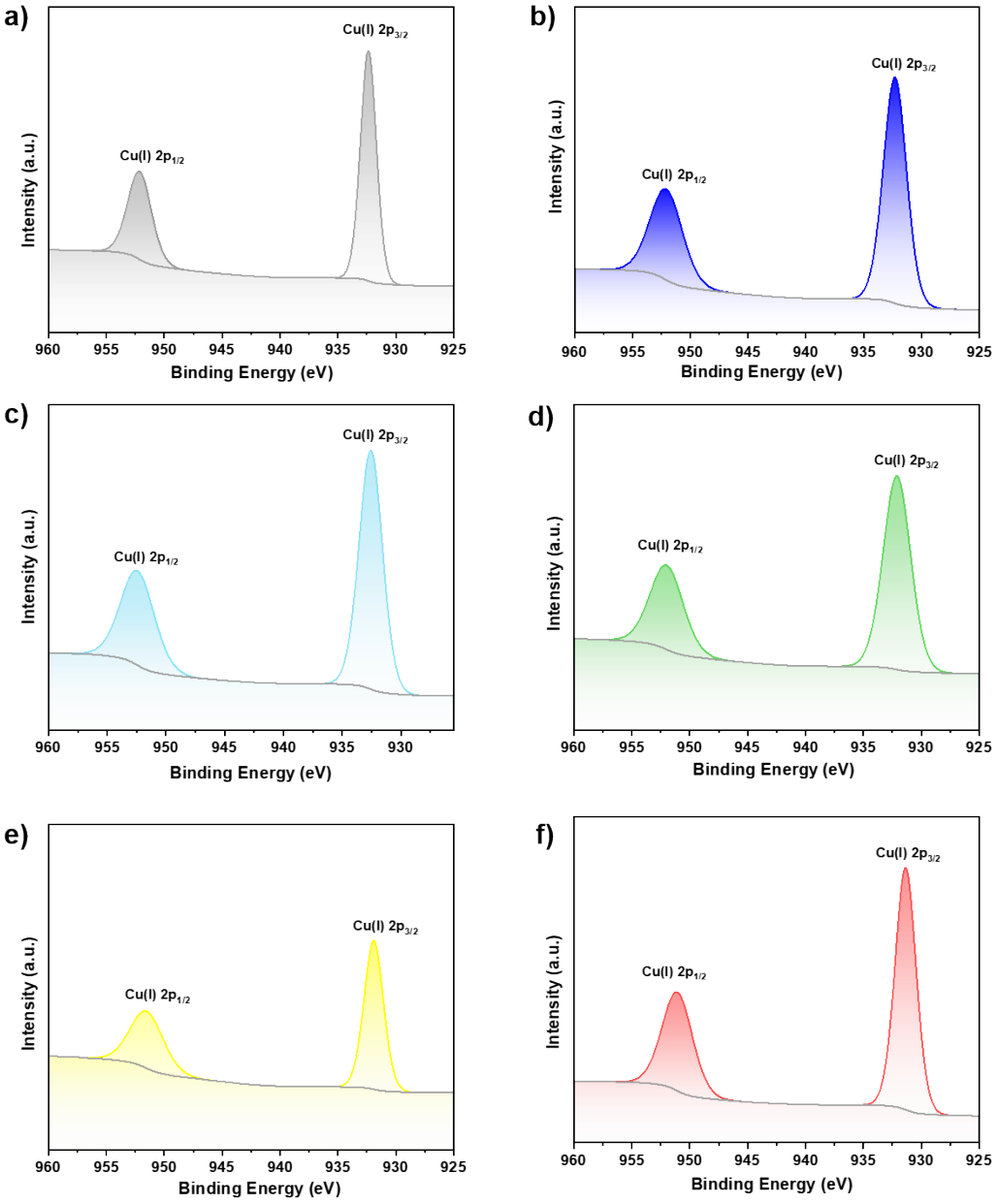

Fig. S3 XPS patterns of a) **N**, b) **B**, c) **C**, d) **G**, e) **Y** and f) **R**.

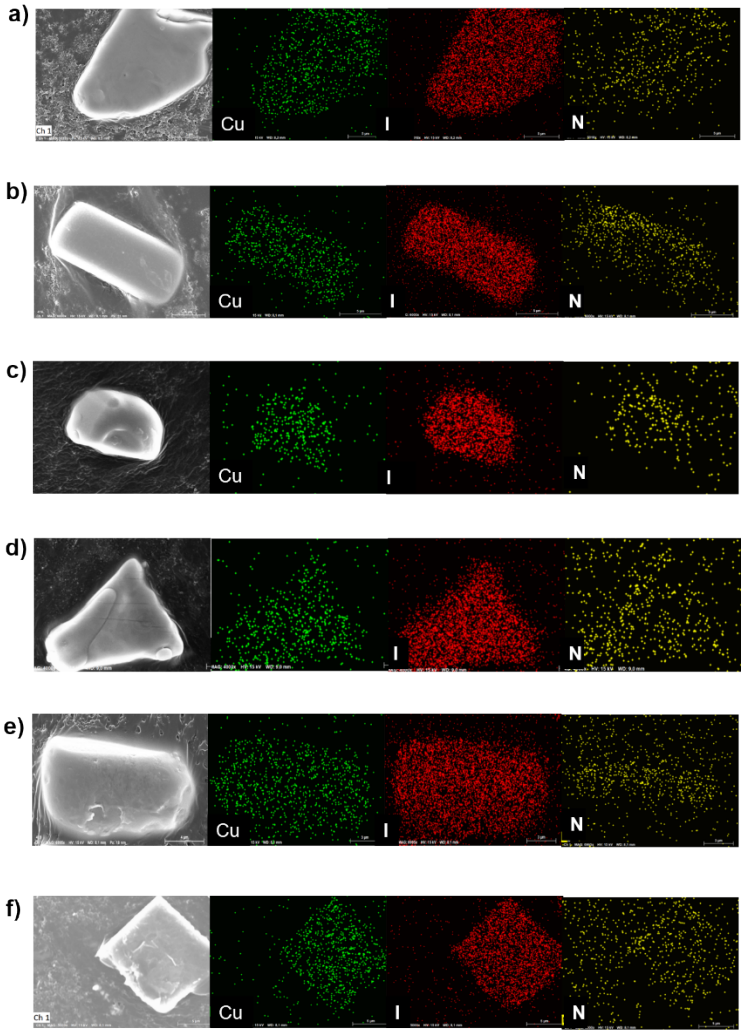

Fig. S4 EDS elemental mappings of Cu, I and N in a) **N**, b) **B**, c) **C**, d) **G**, e) **Y** and f) **R**.

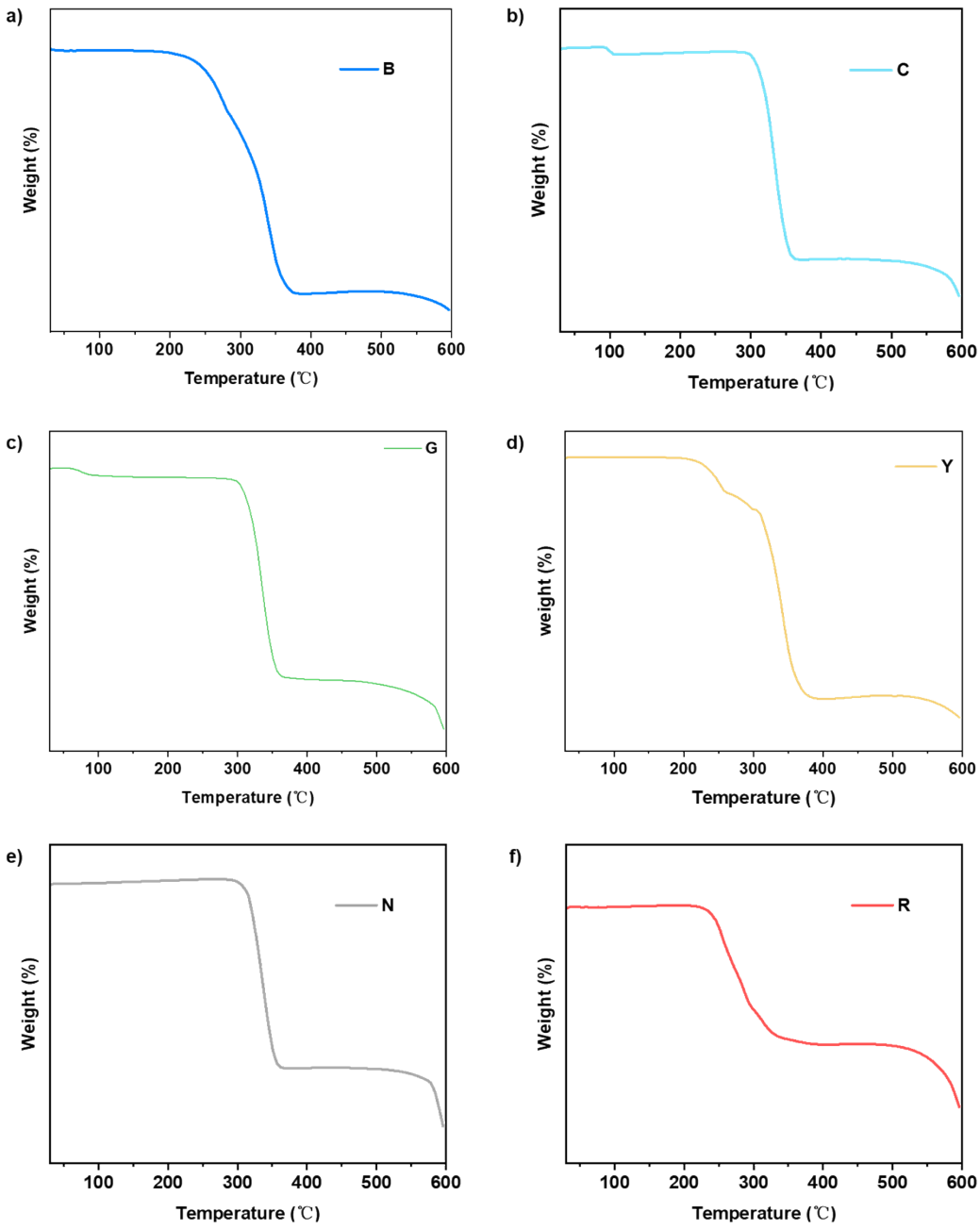

Fig. S5 The TG curves of a) **B**, b) **C**, c) **G**, d) **Y**, e) **N** and f) **R**.

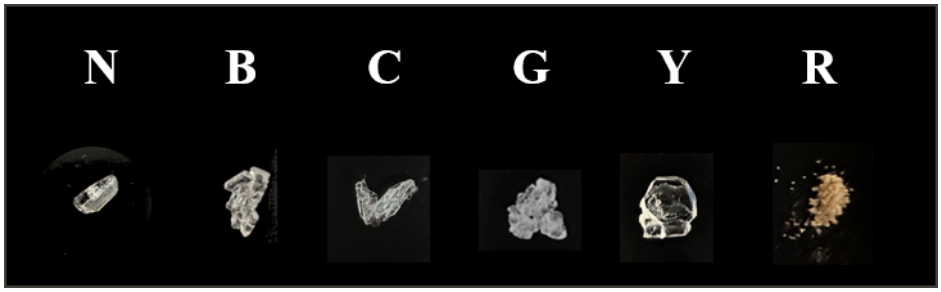

Fig. S6 Photographs of six compounds powders under sunlight.

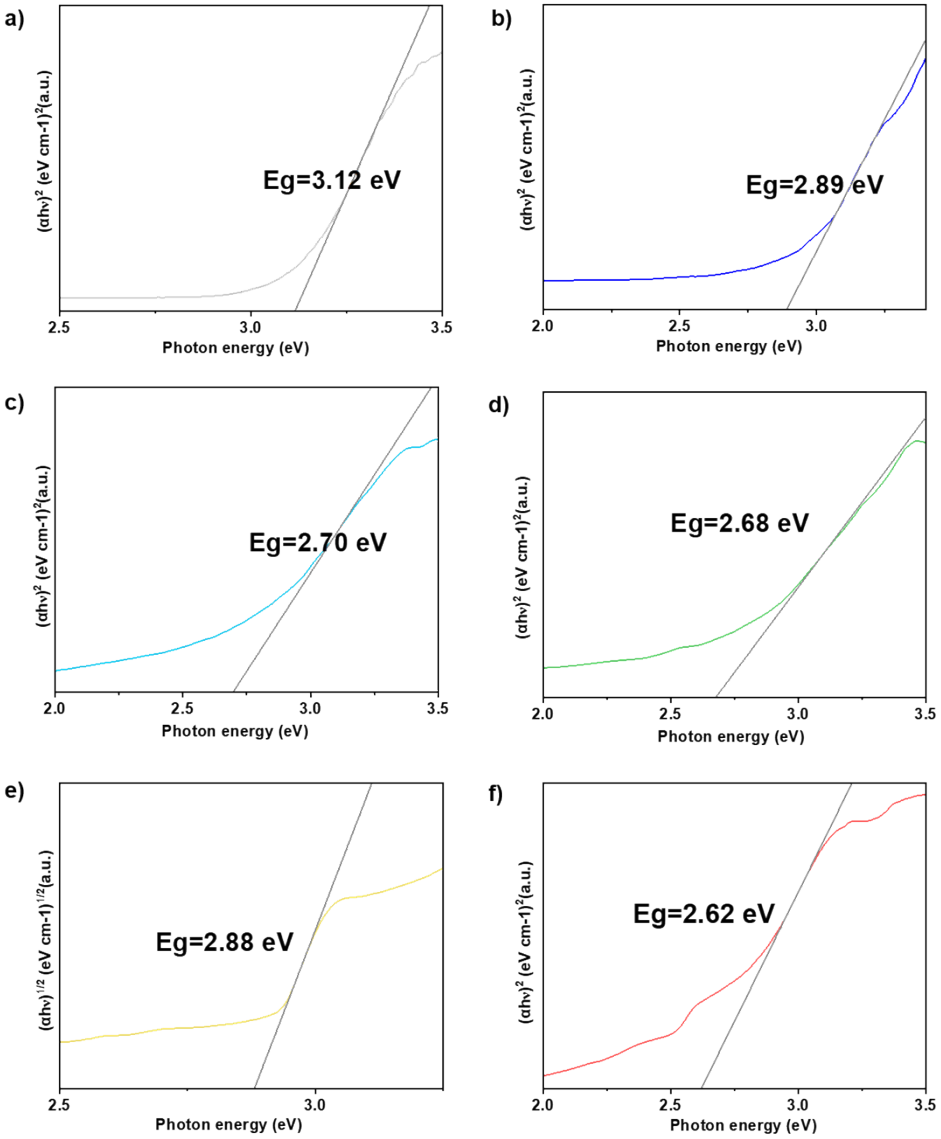

Fig. S7 UV-vis absorption spectra of a) **N**, b) **B**, c) **C**, d) **G**, e) **Y** and f) **R** at room temperature and the corresponding Tauc plot of the absorption spectrum.

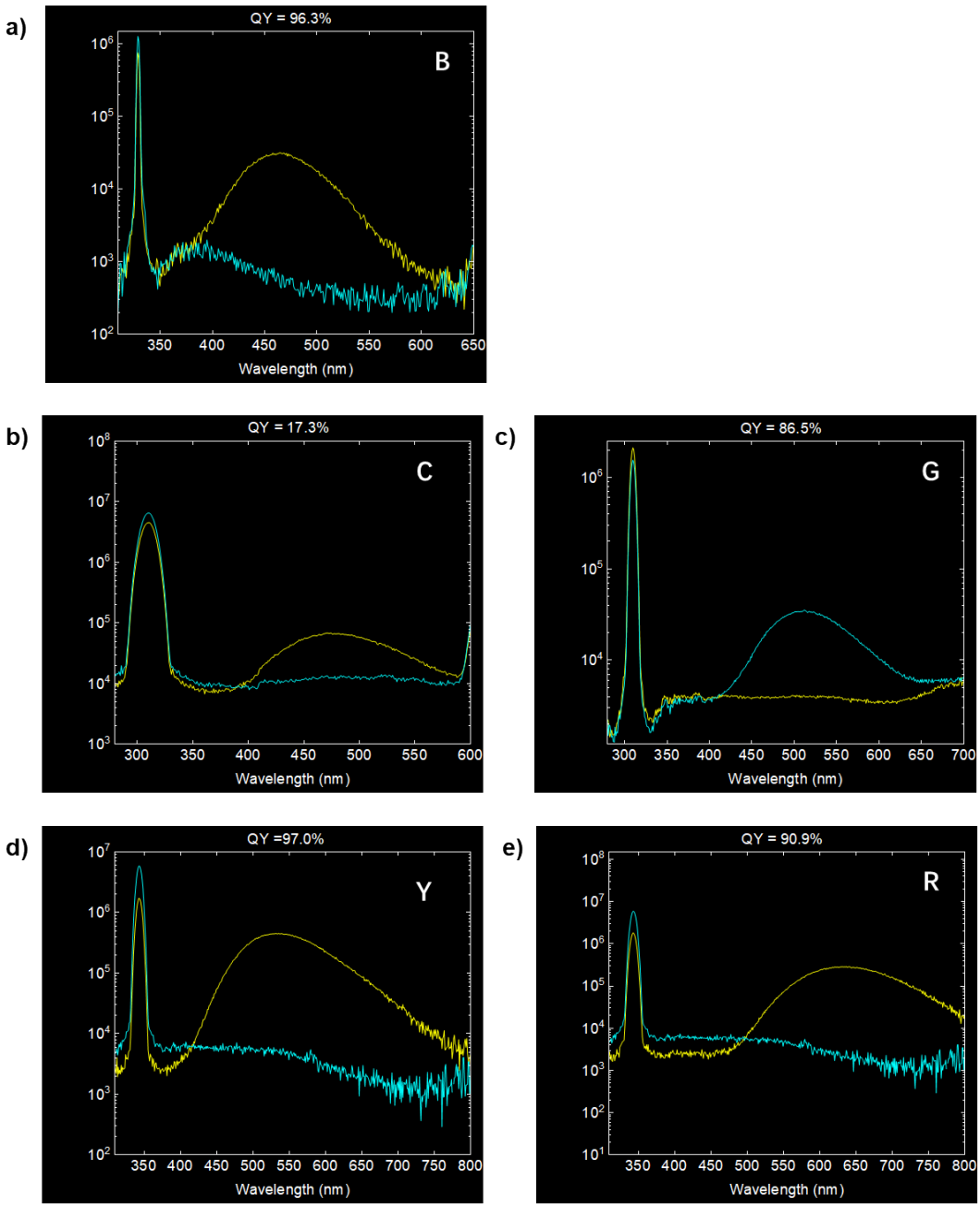

Fig. S8 The photoluminescence quantum yields of **B** (a), **C** (b), **G** (c), **Y** (d) and **R** (e).

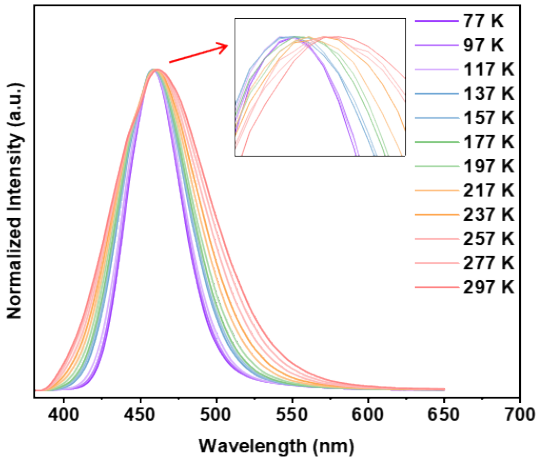

Fig. S9 Temperature-dependent normalized emission spectra of **B** from 77 to 297 K under 254 nm excitation.

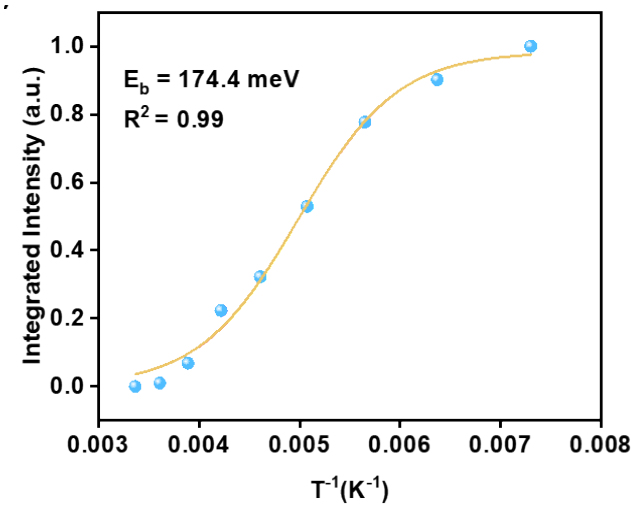

Fig. S10 The exciton binding energy (E_b) values for **B**.

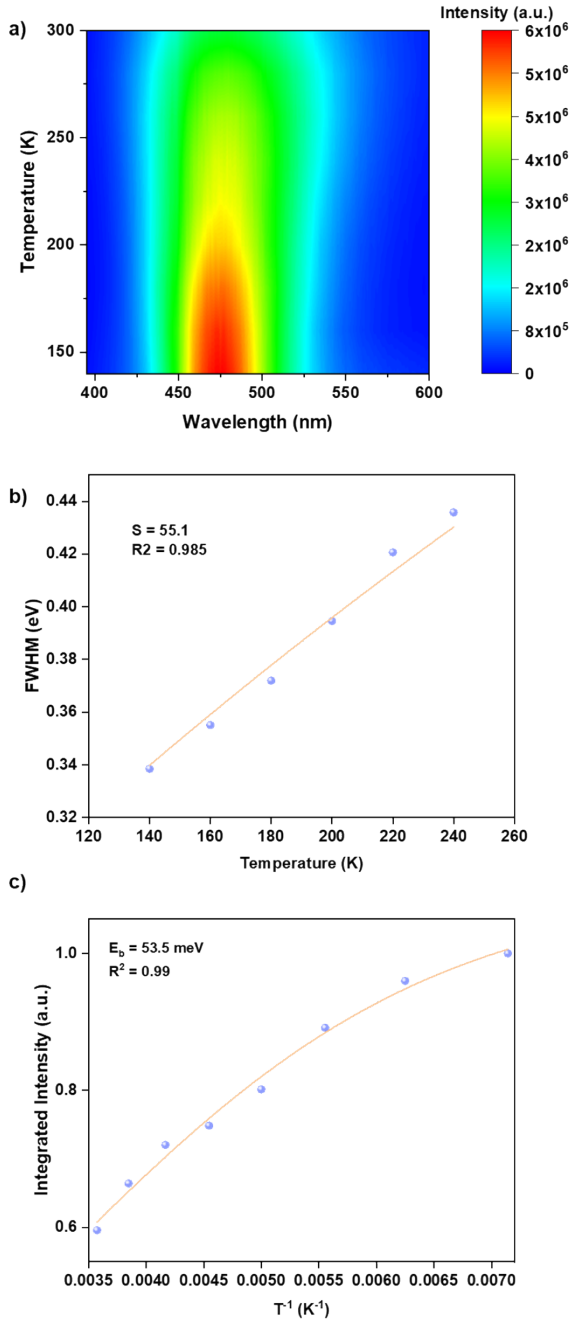

Fig. S11 a) Temperature-dependent PL emission contour mappings of **C.** b) The FWHM of the PL spectra at various temperatures for **C**. c) The exciton binding energy (E_b) values for **C**.

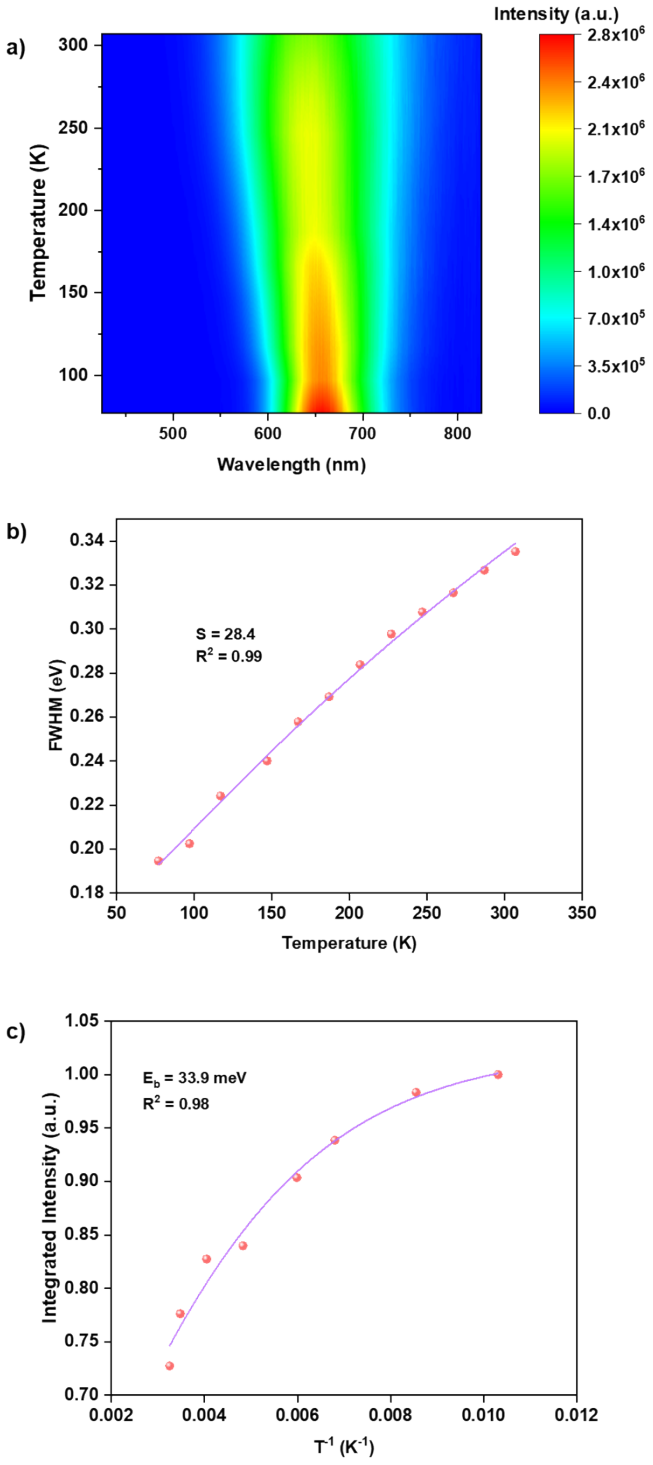

Fig. S12 a) Temperature-dependent PL emission contour mappings of **R.** b) The FWHM of the PL spectra at various temperatures for **R**. c) The exciton binding energy (E_b) values for **R**.

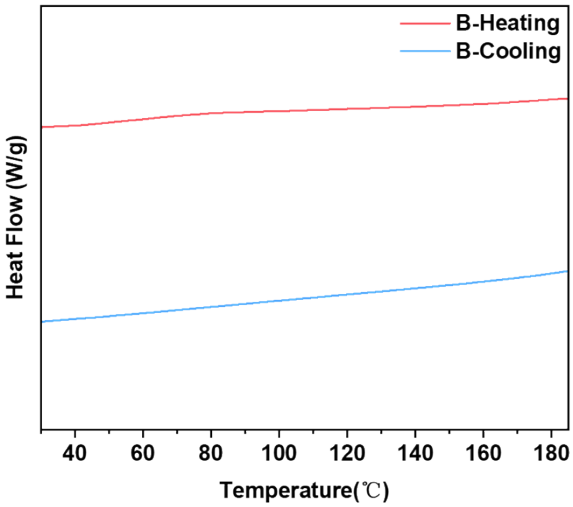

Fig. S13 The DSC curve of **B**.

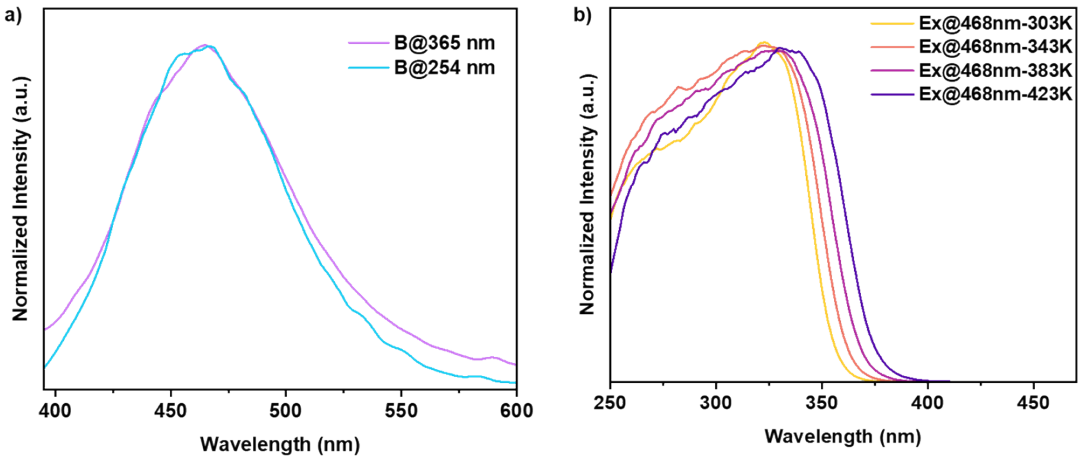

Fig. S14 a) The emission spectra of **B** under excitation at 254 nm and 365 nm. b) High temperature-dependent PLE emission spectra of **B**.

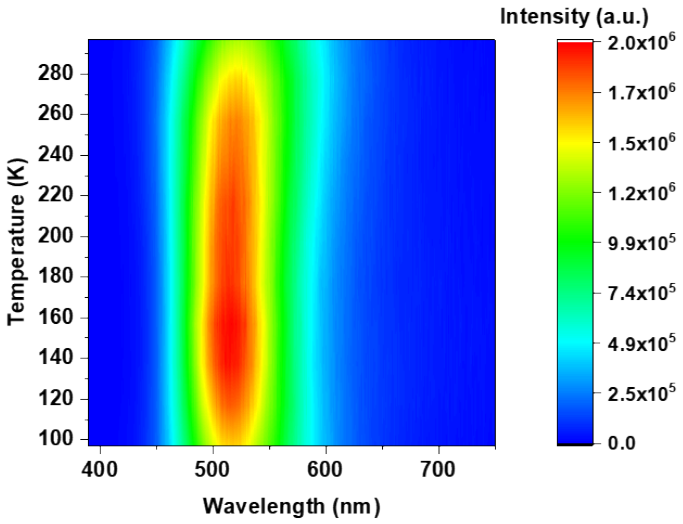

Fig. S15 Temperature-dependent PL emission contour mappings of **G**.

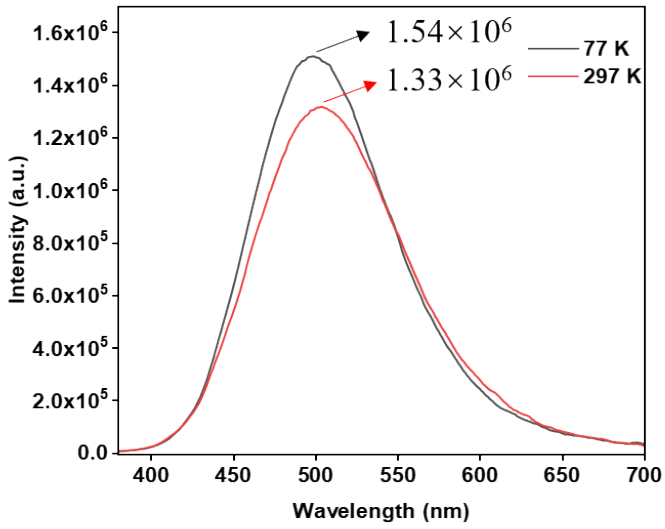

Fig. S16 Comparison of the luminescence intensity of Compound **G** at 77 K and 297 K.

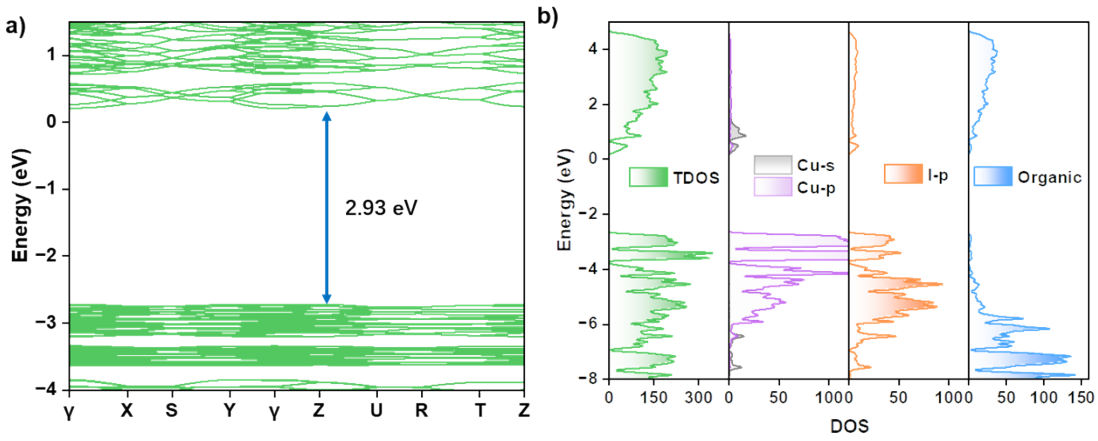

Fig. S17 a) Band structure of **G**. b) Density of states (DOS) of **G**.

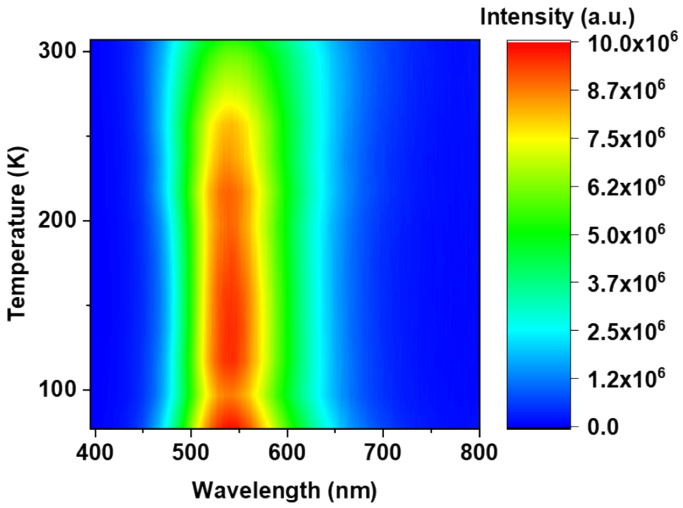

Fig. S18 Temperature-dependent PL emission contour mappings of **Y**.

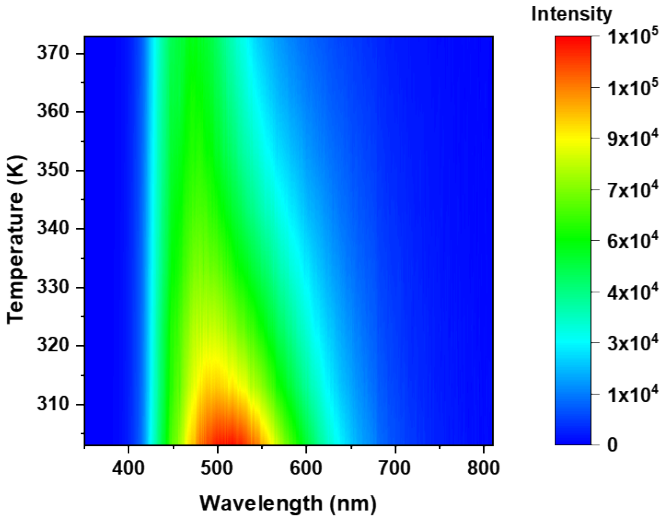

Fig. S19 Temperature-dependent PL emission contour mappings of **Y**.

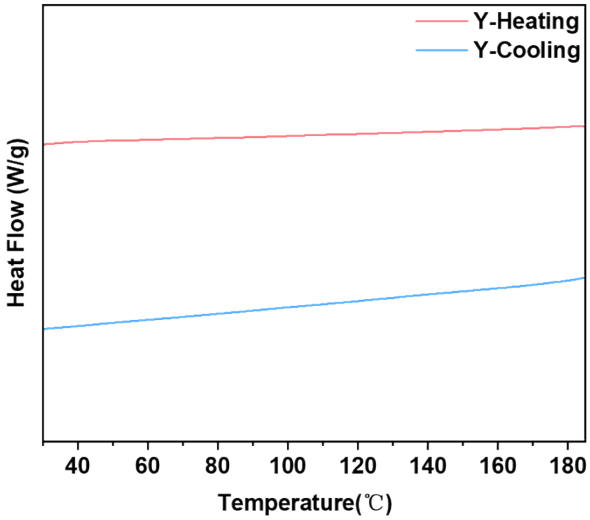

Fig. S20 The DSC curve of **Y**.

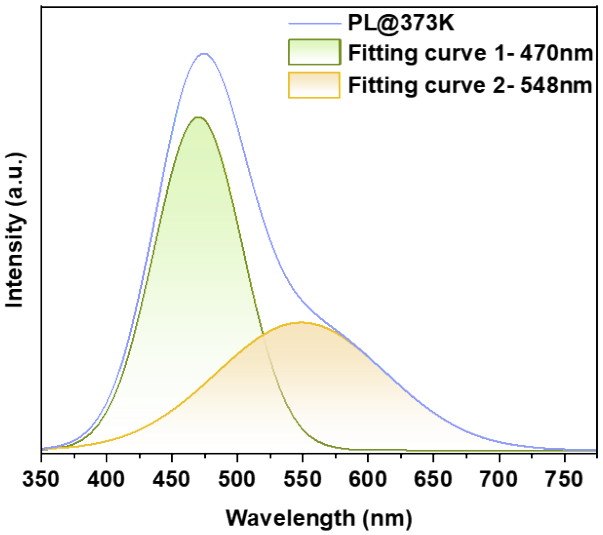

Fig. S21 Peak-differentiating and imitating at 373K of **Y**.

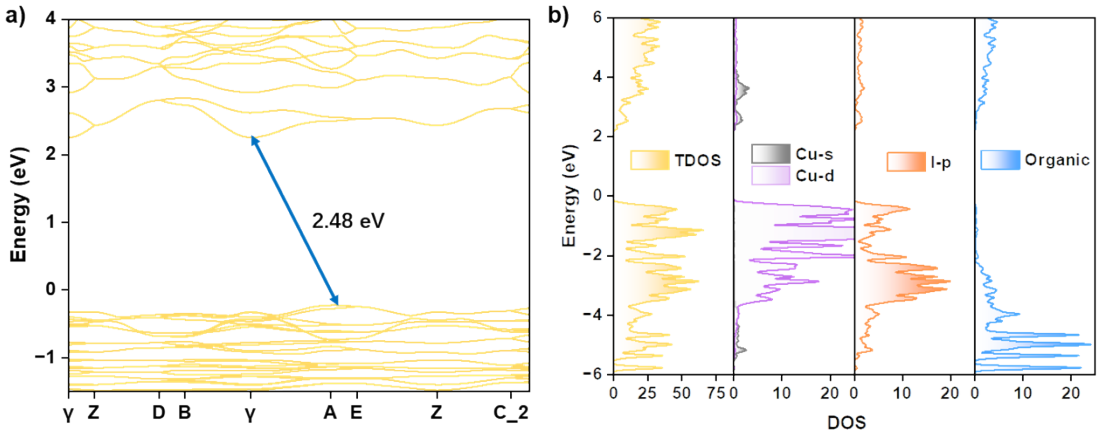

Fig. S22 a) Band structure of **Y**. b) Density of states (DOS) of **Y**.

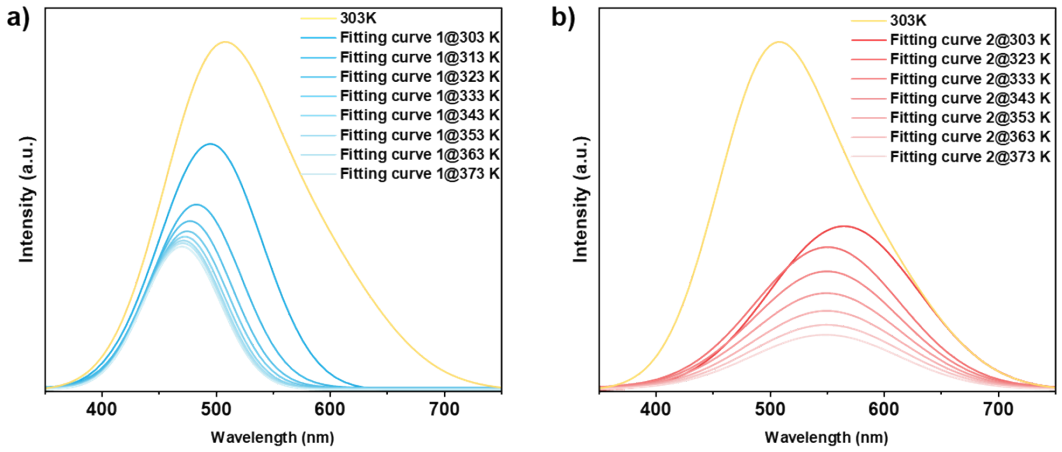

Fig. S23 Gaussian fitting of PL spectra at different temperatures: a) HE emission peak, b) LE emission peak.

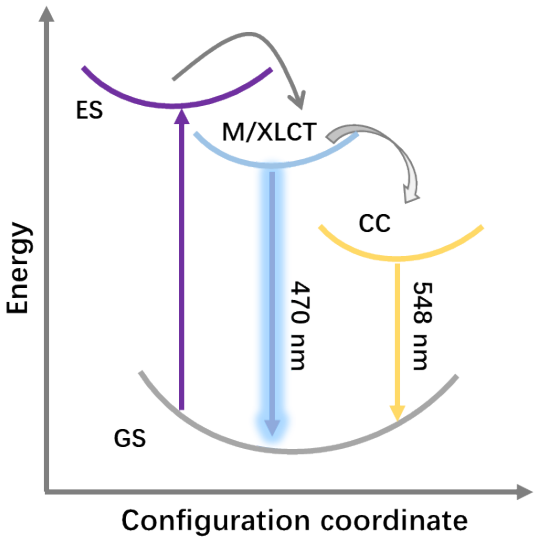

Fig. S24 Proposed mechanism of **Y** at 373K.

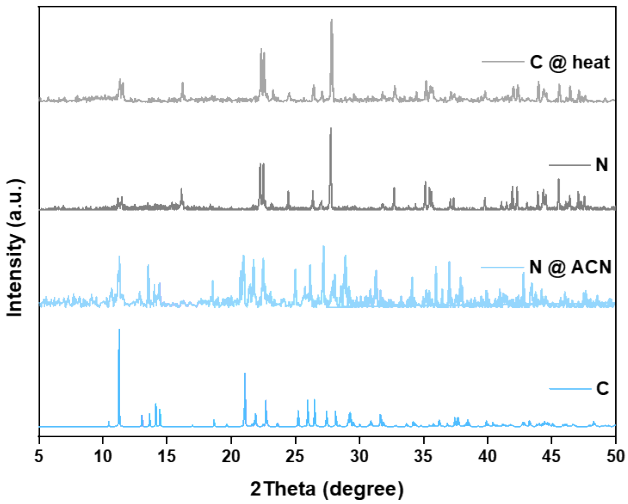

Fig. S25 PXRD patterns of the transformation between **C** and **N**.

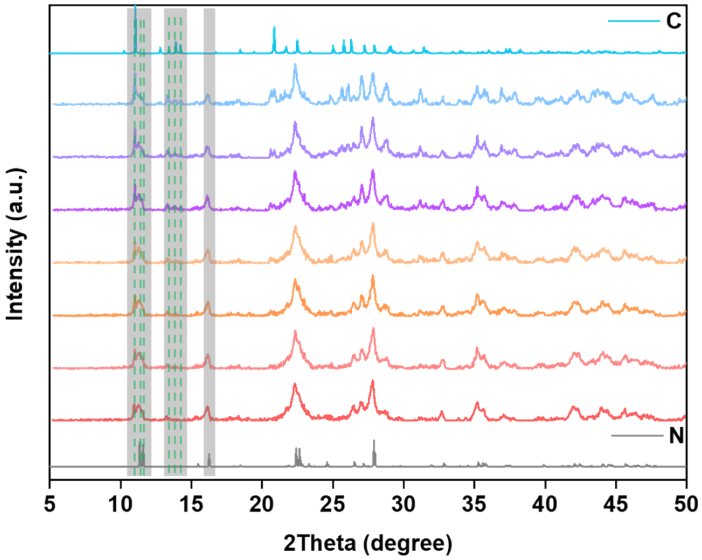

Fig. S26 In situ XRD of the transition from **C** to **N**.

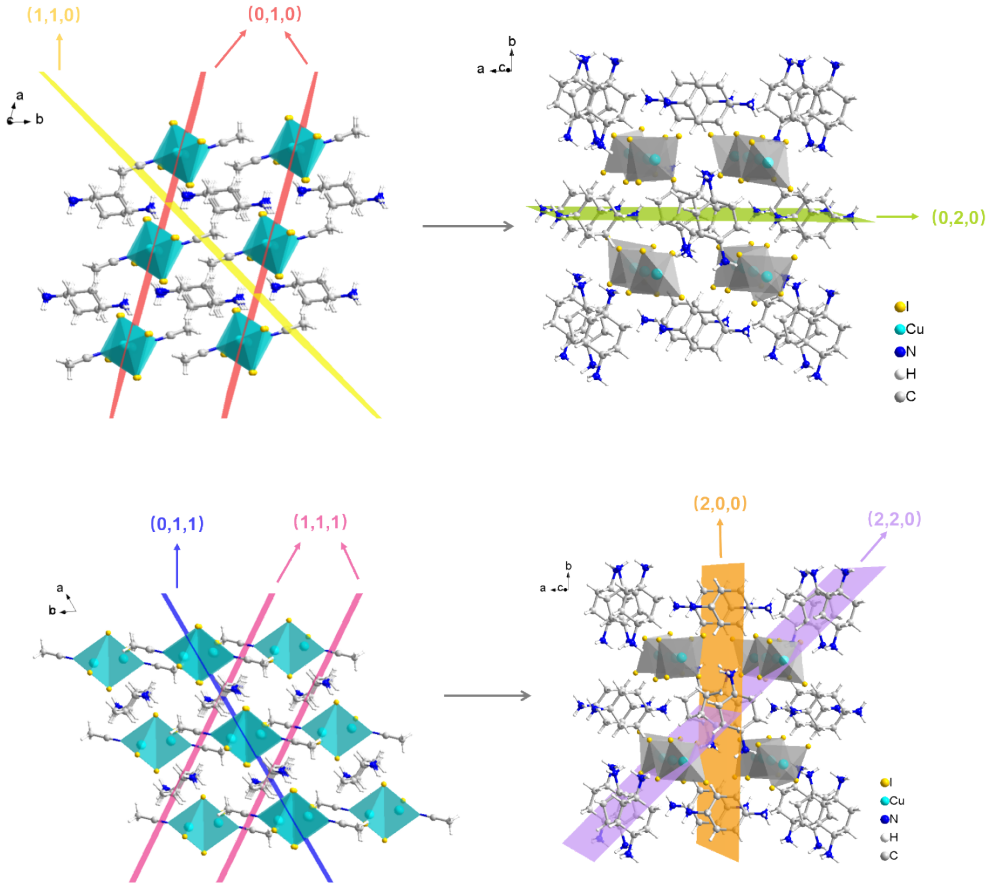

Fig. S27 Crystal plane transformation diagram from **C** to **N**.

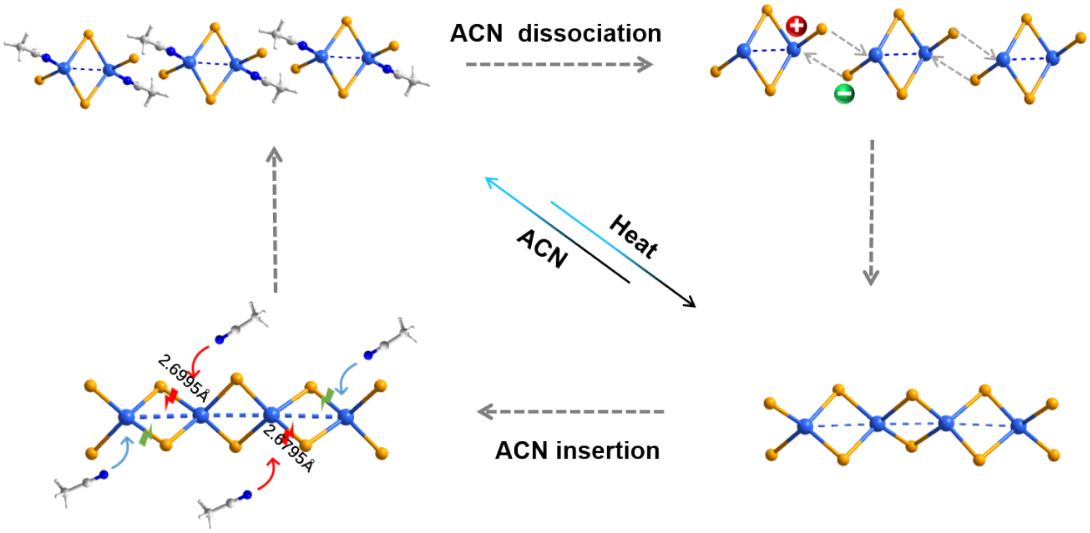

Fig. S28 The transformation diagram of the speculated structures of **C** and **N.**

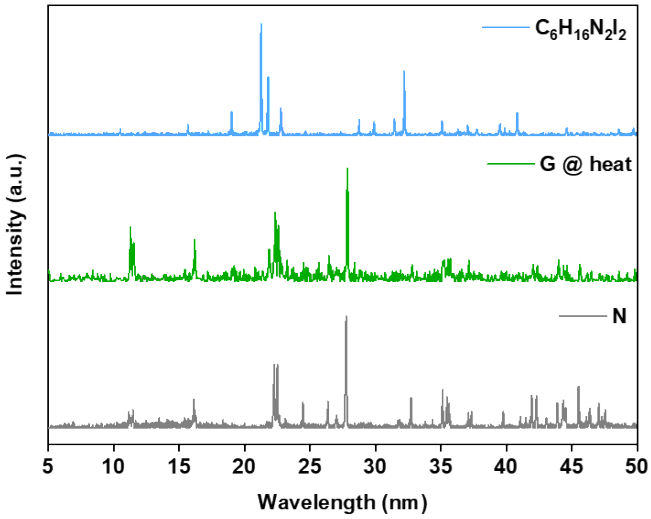

Fig. S29 PXRD patterns of transformation of **G** to **N**.

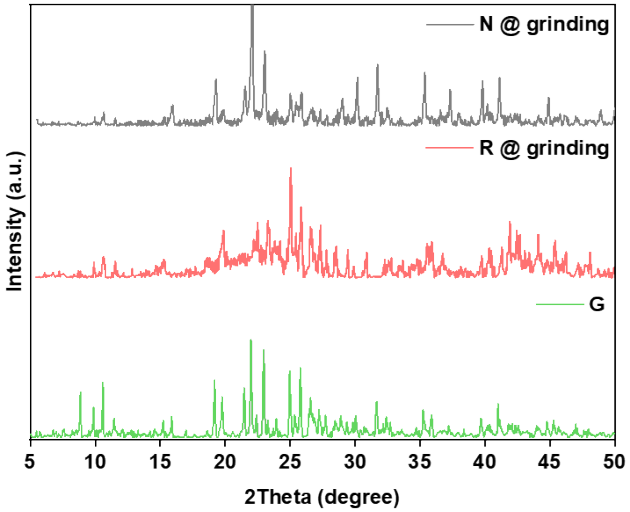

Fig. S30 PXRD patterns of transformation of **N/R** to **G**.

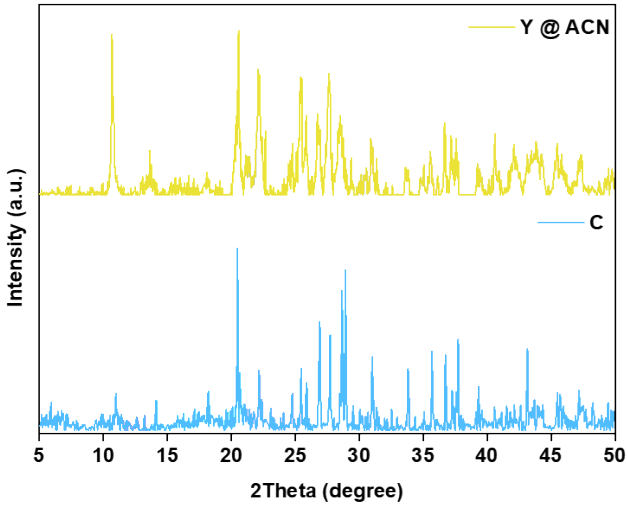

Fig. S31 PXRD patterns of transformation of **Y** to **C**.

Table S10. Letter represented by Senary System.

Senary	decimal base	ASCII
151	67	C
252	104	h
253	105	i
302	110	n
241	97	a

References

1 G. Kresse and J. Furthmüller, Efficiency of Ab-initio Total Energy Calculations for Metals and Semiconductors using A Plane-Wave Basis Set, *Comput. Mater. Sci.*, 1996, **6**, 15-50.

2 V. Wang, N. Xu, J.-C. Liu, G. Tang and W.-T. Geng, VASPKIT: A User-Friendly Interface Facilitating High-Throughput Computing and Analysis using VASP Code, *Comput. Phys. Commun.*, 2021, **267**, 108033.

3 J. P. Perdew, M. Ernzerhof and K. Burke, Rationale for Mixing Exact Exchange with Density Functional Approximations, *J. Chem. Phys.*, 1996, **105**, 9982-9985.

4 N. Lin, L. Xiao, Y. Wu, Y.-F. Wu, Z.-X. Li, T.-Y. Yan, Z.-W. Chen, C.-Y. Yue, D. Yan and X.-W. Lei, 2D Cuprous Halide Scintillator with Dual Excitation-Dependent and Thermochromic Luminescence toward Multifunctional Optoelectronic Applications, *Adv. Mater.*, 2025, **37**, e01560.

5 S. Cao, J. a. Lai, Y. Wang, K. An, T. Jiang, M. Wu, P. Feng, P. He and X. Tang, Organic-Inorganic Cuprous Halides With Reversible Photoluminescence for Multiple Optical Applications, *Laser Photon. Rev.*, 2024, **18**, 2400799.

6 R. An, Q. Wang, Y. Liang, P. Du, P. Lei, H. Sun, X. Wang, J. Feng, S. Song and H. Zhang, Reversible Structural Phase Transitions in Zero-Dimensional Cu(I)-Based Metal Halides for Dynamically Tunable Emissions, *Angew. Chem. Int. Ed.*, 2025, **64**, e202413991.